1T Phase as an Efficient Hole Injection Layer to TMDs Transistors: A Universal Approach to Achieve p-type Contacts

Xiaohui Hu,[*1,2] Yifeng Wang,[1,2] Xiaodong Shen,[1,2] Arkady V. Krasheninnikov,[3,4]

Litao Sun,[*5] Zhongfang Chen[*6]

[1] College of Materials Science and Engineering, Nanjing Tech University, Nanjing 210009, China

[2] Jiangsu Collaborative Innovation Center for Advanced Inorganic Function Composites, Nanjing Tech University, Nanjing 210009, China

[3] Institute of Ion Beam Physics and Materials Research, Helmholtz-Zentrum Dresden-Rossendorf, 01314 Dresden, Germany

[4] Department of Applied Physics, Aalto University School of Science, PO Box 11100, 00076 Aalto, Finland

[5] SEU-FEI Nano-Pico Center, Key Laboratory of MEMS of Ministry of Education, Collaborative Innovation Center for Micro/Nano Fabrication, Device and System, Southeast University, Nanjing 210096, China

[6] Department of Chemistry, University of Puerto Rico, Rio Piedras Campus, San Juan, Puerto Rico 00931

Corresponding Author:

xiaohui.hu@njtech.edu.cn (XH); slt@seu.edu.cn (LS); zhongfangchen@gmail.com (ZC)

Abstract

Recently, the fabricated MoS_2 FETs with 1T-MoS_2 electrodes exhibit excellent performance with rather low contact resistance, as compared with those with metals deposited directly on 2H-MoS_2 [*Nat. Mater.* **2014**, *13*, 1128], but the reason for that remains elusive. By means of density functional theory calculations, we investigated the carrier injection at the 1T/2H MoS_2 interface and found that although the Schottky barrier height (SBH) values of 1T/2H MoS_2 interfaces can be tuned by controlling the stacking patterns, the p-type SBH values of 1T/2H MoS_2 interfaces with different stackings are lower than their corresponding n-type SBH values, which demonstrated that the metallic 1T phase can be used as an efficient hole injection layer for 2H-MoS_2. In addition, as compared to the n-type Au/MoS_2 and Pd/MoS_2 contacts, the p-type SBH values of 1T/2H MoS_2 interfaces are much lower, which stem from the efficient hole injection between 1T-MoS_2 and 2H-MoS_2. This can explain the low contact resistance in the MoS_2 FETs with 1T-MoS_2 electrodes. Notably, the SBH values can be effectively modulated by an external electric field, and a significantly low p-type SBH value can be achieved under an appropriate electric field. We also demonstrated that this approach is also valid for WS_2, WSe_2 and $MoSe_2$ systems, which indicates that the method can most likely be extended to other TMDs, and thus may open new promising avenues of contact engineering in these materials.

Introduction

Two-dimensional (2D) transition metal dichalcogenides (TMDs) have recently received great attention as the channel material for field effect transistors (FETs) [1–8]. In principle, TMD FETs can transport either electrons (n-FET) or holes (p-FET) in the conducting channel, depending on the height of the Schottky barrier relative to the conduction band minimum (CBM) or valence-band maximum (VBM) [9]. However, most experimentally reported TMD FETs based on a Schottky device architecture are of n-type probably due to the relative ease of fabrication [9–12]. To complement TMDs for digital logic applications, it is highly desirable to develop p-type TMD-based FETs [13]. However, the studies of p-type TMD FETs are rather scarce due to the fabrication difficulties [9]. Thus, significant efforts have been undertaken to achieve efficient hole contacts. Experimentally, p-type multilayer MoS_2 FETs have been manufactured through hole-doping by palladium (Pd) contacts in the limit of large gate fields [14]. Recently, molybdenum trioxide (MoO_x, $x < 3$) [9, 15], a high work function material, was used as a buffer layer between Pd and MoS_2/WSe_2, and showed an efficient hole injection to MoS_2 and WSe_2. In particular, FETs made from single-layer MoS_2, a semiconductor with a direct band gap of 1.8 eV [1, 16], high carrier mobility (~200cm^2/Vs) and excellent on/off current ratio (10^8) [17], demonstrate appealing performance. According to recent density functional theory (DFT) calculations [18–20], various metals can contact with MoS_2 to form n-type transistors, since the Fermi level of elemental metals is pinned close to the CBM of MoS_2. In stark contrast, among numerous metals examined (including Al, Ag, Au, Pd,

Ir, Pt, Ru, Ni, Sc and Ti), only in the case of platinum, a p-type Schottky contact was computationally identified at the Pt/MoS_2 interface [18, 20]. In addition, graphene oxide (GO) was proposed to be a promising hole injection layer for single-layer MoS_2 due to its high work function and the relatively weak Fermi level pinning at the interfaces, and the p-type SBH can be decreased significantly by increasing the oxygen concentration as well as the fraction of epoxy functional groups in GO [21]. However, GO is nonstoichiometric, and it is rather challenging to experimentally control the oxygen concentration and the epoxy to hydroxyl ratio [22].

Monolayer TMDs have three polymorphs, namely trigonal prismatic (2H), octahedral (1T), and distorted 1T(1T') [23], among which the semiconducting 2H phase is energetically most favorable and has the highest stability. The phase transformations from the 2H-MoS_2 to the metallic 1T-MoS_2 can be induced by electron beam [24, 25] or lithium or sodium ion intercalation [26, 27]. Note that 1T-MoS_2 can exist even after complete removal of the ion support, although this phase is stabilized by electron donation via ion intercalation during synthesis [28, 29]. Recent experiments clearly demonstrated the advantages of 1T-MoS_2 over 2H-MoS_2 for some applications: 1T-MoS_2 shows higher catalytic activity for hydrogen evolution reactions (HER) [30, 31]. Especially, Kappera *et al*. found that, as compared with those with metals deposited directly on 2H-MoS_2, FETs with locally introduced 1T-MoS_2 (with ~70% concentration) electrodes exhibited superior performance with rather low contact resistance, and expected that the FETs with pure 1T phase could have even greater enhancement in performance [27, 32]. Then, a

question raises naturally, why do MoS_2 FETs with 1T phase electrodes exhibit excellent performance? How does the carrier injection occur at the 1T/2H MoS_2 interface? Can such an approach be extended to other TMDs?

In this work, by means of systematic DFT calculations, we studied the carrier injection at the 1T/2H MoS_2 interface and demonstrated that the metallic 1T phase can be used as an efficient hole injection layer for 2H-MoS_2. We show that 1T-MoS_2 forms a p-type contact with 2H-MoS_2, and the p-type SBH values are lower than those of the n-type Au/MoS_2 and Pd/MoS_2 contacts [18], which stem from the efficient hole injection between 1T-MoS_2 and 2H-MoS_2. This can explain the low contact resistance in the MoS_2 FETs with 1T-MoS_2 electrodes [27]. Notably, we find that an external electric field is able to effectively modulate the band alignment of 1T/2H MoS_2 interfaces, and the SBH values can be reduced or enhanced depending on the magnitude and direction of the electric field, and a significantly low p-type SBH value can be achieved under an appropriate electric field. Finally, we extend our studies to other TMDs, such as WS_2, WSe_2 and $MoSe_2$, and find that the p-type contacts are also obtained in their 1T/2H interfaces.

Computational Method

Our DFT calculations were performed using the VASP package [33, 34]. The projector-augmented-wave (PAW) method was employed to describe electron-ion interactions [35, 36], while the exchange-correlation functional was treated by generalized gradient approximation (GGA) in the scheme of Perdew-Burke-Ernzerhof (PBE) [37]. Van der Waals corrections were included through Grimme's DFT-D2

method as implemented in VASP [38, 39]. The energy cutoff of the plane wave was set to 500 eV, and the atomic positions were fully relaxed until the maximum force on each atom was less than 0.005 eV/Å. A k-point sampling of 32 × 32 × 1 was used for geometry optimizations and self-consistent calculations, and a vacuum region of 16 Å was introduced to avoid interaction between periodic images of slabs. Note that in DFT calculations, 1T phase can spontaneously transform into the 1T'-MoS_2 [40], but the difference between these two phases is rather small. Moreover, 1T phase was experimentally synthesized [27, 32]. Thus, in this work we adapted the 1T-MoS_2 phase instead of 1T'-MoS_2, as it gives the qualitatively correct picture and the computed SBH trends are not affected (see figures S1, S2 and the related text in Supporting Information). In addition, the spin–orbit interactions were not accounted here, as it does not affect the p-type SBH trends (see figure S3 in the Supporting Information for details).

Results and discussion

In order to construct the 1T/2H MoS_2 interfaces, we first examined the lattice constants of 1T-MoS_2 and 2H-MoS_2 monolayers. The calculated lattice constants of 1T and 2H phases of MoS_2 are the same (3.18Å), well consistent with previous results [41]. Thus, the 1T/2H MoS_2 interfaces can be constructed simply by stacking the primitive cells of 1T-MoS_2 and 2H-MoS_2 without any strain. Note that there are three high-symmetry sites in monolayer 2H-MoS_2: S-site (denoted as A), Mo-site (B), and center-of-hexagon (C). All the 1T/2H MoS_2 interfaces can be built using these sites. For example, as shown in figure 1(a), monolayer 2H-MoS_2 can be named as ABA,

while monolayer 1T-MoS_2 is denoted as ABC according to the atomic stacking sequence (S'-Mo-S). For all the 1T/2H MoS_2 interfaces in this work, the bottom layer is always 2H-MoS_2 (ABA), while the top 1T-MoS_2 layer has totally six different atomic sequences when stacked above 2H-MoS_2, namely ABC, ACB, BAC, BCA, CAB and CBA (Figure 1(a)-1(f)). Because one layer is always 2H-MoS_2 (ABA), for simplicity, we used the atomic stacking sequence of 1T-MoS_2 to name these six different stackings of 1T/2H MoS_2 (Figure 1).

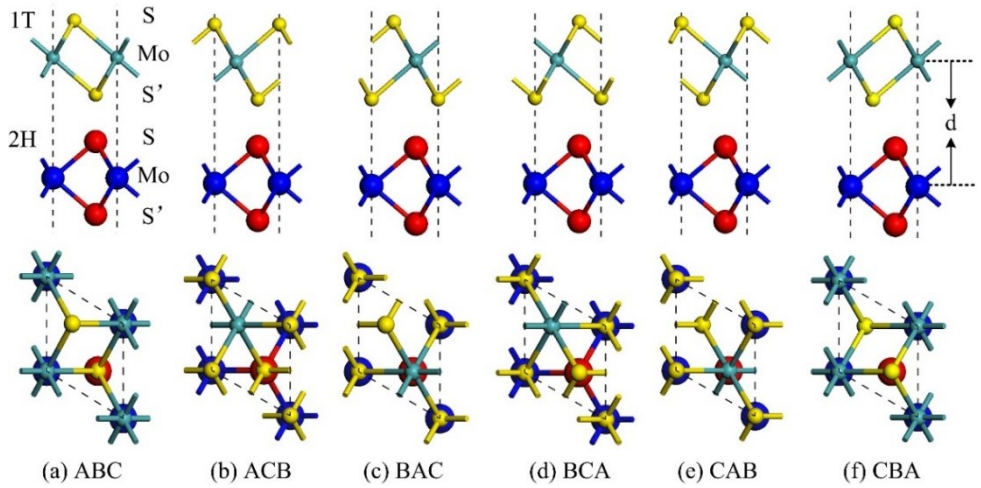

Figure 1. The top and side views of six different stackings of 1T and 2H MoS_2 sheets. The definition for the interlayer distance *d* is indicated in panel (f).

To investigate the stability of the 1T/2H MoS_2 interfaces, we computed the interlayer binding energy, which is defined as the energy difference between 1T/2H MoS_2 and the corresponding monolayers ($E_b = E_{1T/2H} - E_{1T} - E_{2H}$) (see the related text in Supporting Information). According to this definition, a more negative E_b value indicates a higher stability of the interface. As summarized in Table 1, the interlayer

binding energies of ABC and ACB stacked 1T/2H MoS_2 (-0.10 eV) are slightly less negative than those of BAC, BCA, CAB and CBA stacked 1T/2H MoS_2 (-0.15~-0.17 eV), which indicates that the ABC and ACB stacked 1T/2H MoS_2 are less favorable than the others. Overall, all the interlayer binding energies are negative, suggesting that all these 1T/2H MoS_2 interfaces are energetically favorable.

The interfacial distances well correlate with the interlayer binding energies for 1T/2H MoS_2 interfaces. Specifically, the interfacial distance *d* is significantly larger in the energetically less favorable ABC and ACB stacked 1T/2H MoS_2 (6.83 and 6.75 Å, respectively) than other stackings (6.14~6.24Å). Note that the equilibrium distance between monolayer 2H-MoS_2 and 1T-MoS_2 depends on the relative position of S atoms at the interface. When S atoms at the interface are stacked directly on top of each other, the interlayer coupling between the two monolayers is weaker, leading to the increased interlayer distance and less favorable binding energy for ABC and ACB stacked 1T/2H MoS_2. In contrast, when S atoms at the interface are staggered, the interlayer coupling becomes stronger, leading to a decreased interlayer distance and stronger binding energy in BAC, BCA, CAB and CBA stacked 1T/2H MoS_2 (Table1).

Table 1. The interlayer binding energy E_b (eV/f.u.), the equilibrium interfacial distance d (Å) between the 1T-MoS_2 Mo plane and the 2H-MoS_2 Mo plane, the n-type SBH values (n-SBH), and the p-type SBH values (p-SBH) in the 1T/2H MoS_2 interfaces.

	E_b (eV/f.u.)	d (Å)	n-SBH (eV)	p-SBH (eV)
ABC	-0.10	6.83	0.81	0.67
ACB	-0.10	6.75	0.83	0.65
BAC	-0.17	6.24	0.79	0.49
BCA	-0.16	6.14	0.70	0.48
CAB	-0.16	6.19	0.82	0.44
CBA	-0.15	6.23	0.75	0.49

The electronic properties of 2H-MoS_2 and 1T-MoS_2 are quite different. At the PBE level of theory, 2H-MoS_2 is semiconducting with a direct band gap of 1.68 eV, while 1T-MoS_2 is metallic (figure S4, Supporting Information). Our results agree well with previous theoretical calculations [41]. SBH is a key factor that determines contact resistances in the MoS_2 transistors [42]. According to previous DFT simulations on GO/MoS_2 interfaces [21] and metal/MoS_2 contacts [18], the n-type SBH is defined as the energy difference between the Fermi level of the interfaces and the CBM of 2H-MoS_2 layer, while the p-type SBH is the energy difference between the VBM of 2H-MoS_2 layer and the Fermi level of the interfaces. Therefore, we computed the band structures (Figure 2(a)-(f)), the total density of states (TDOS) of the 1T/2H

MoS_2 interfaces and the projected density of states (PDOS) from 2H-MoS_2, 1T-MoS_2 of the interfaces (figure S5, Supporting Information), then obtained the SBH values by comparing the band structures and DOS of the interfaces with those of 2H-MoS_2 from the interfaces. To gain further insight, we carefully checked the band alignment for monolayer 2H-MoS_2, monolayer 1T-MoS_2 and 1T/2H MoS_2 interfaces (Figure 2(g)), and found that the work function ($W = E_{vac} - E_F$, where E_{vac} and E_F are the vacuum level and Fermi level, respectively) of 1T-MoS_2 is closer to the VBM than to the CBM of 2H-MoS_2, indicating that 1T-MoS_2 can be used as a hole contact for 2H-MoS_2. Meanwhile, the Fermi level slightly shifts up after 2H-MoS_2 and 1T-MoS_2 form the 1T/2H MoS_2 interfaces. Thus, the work function of the 1T/2H MoS_2 interfaces is slightly smaller than that of monolayer 2H-MoS_2 and monolayer 1T-MoS_2 (Figure 2(g)).

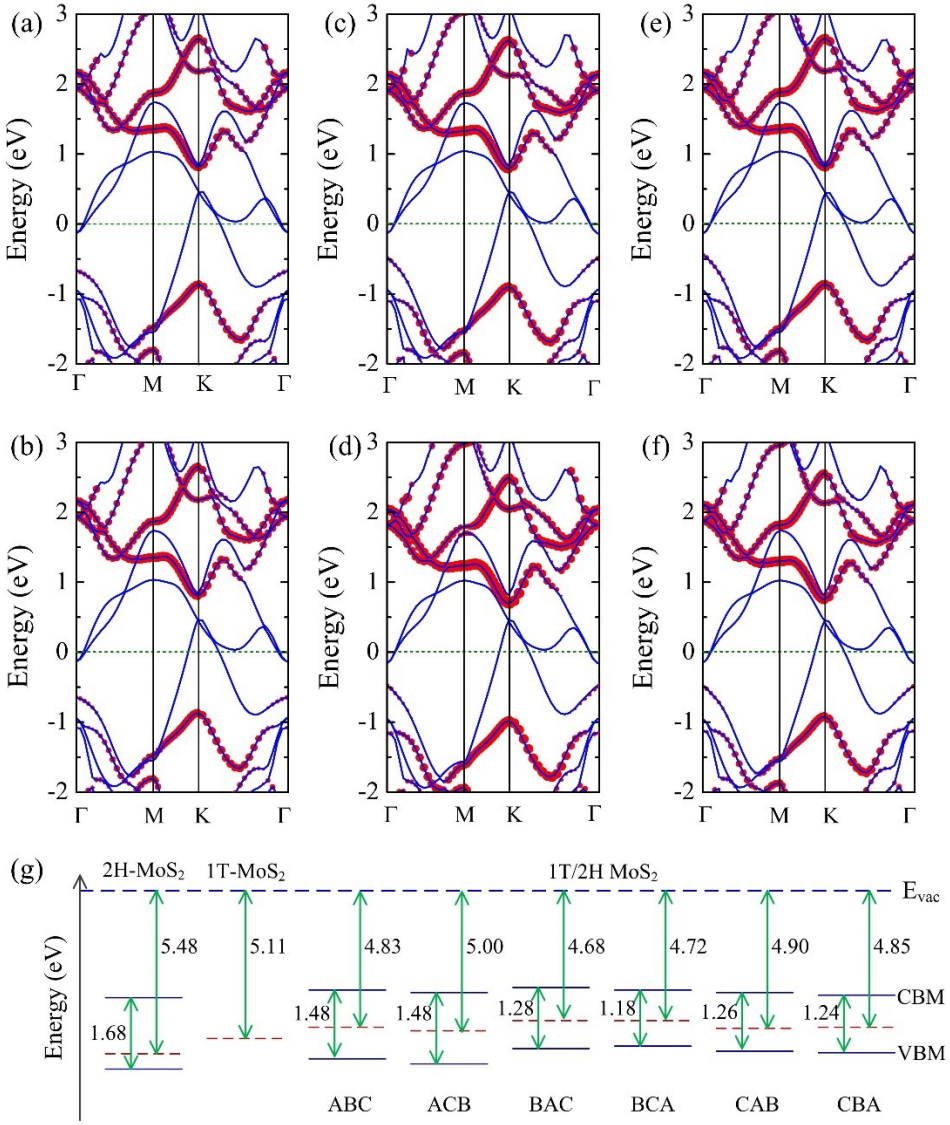

Figure 2. Band structures of 1T/2H MoS_2 interfaces with different stackings of (a) ABC, (b) ACB, (c) BAC, (d) BCA, (e) CAB, and (f) CBA, respectively. The blue solid lines are the overall band structures. The red dots denote the projected band structures of the 2H-MoS_2 layer. The weight is represented by the dot size. The Fermi level is set at zero, indicated by the olive dashed lines. (g) Band alignments of monolayer 2H-MoS_2, monolayer 1T-MoS_2 and 1T/2H MoS_2 interfaces. Relevant electronic parameters are also given. The red dashed lines are the Fermi level. The vacuum level is taken as reference.

Table 1 summarizes the computed n-type and p-type SBH values of the 1T/2H MoS_2 interfaces with different stacking configurations. Notably, the maximal difference in the n-type SBH is 0.13 eV, while that in the p-type SBH is 0.23 eV. Thus, there is a partial Fermi level pinning behavior at the interface, in other words, the Fermi levels are in a 0.13-0.23 eV window in the gap for these six interfacial configurations. Our computations also suggest that the SBH values at the 1T/2H MoS_2 interfaces can be tuned by controlling the stacking patterns.

Interestingly, distinct from most metal/MoS_2 contacts [18], the Fermi level is closer to the VBM than to the CBM of 2H-MoS_2 (Figure 2), indicating that all these 1T/2H MoS_2 interfaces form p-type contacts. Furthermore, the p-type SBH values (0.44–0.67 eV) are lower than those of the n-type Au/MoS_2 and Pd/MoS_2 contacts (0.88 and 0.85 eV, respectively) [18], which result from the efficient hole injection between 1T-MoS_2 and 2H-MoS_2. This can explain the low contact resistance in the MoS_2 FETs with 1T phase electrodes [27]. Note that Au and Pd are the most common electrode materials, and were also used in Kappera's studies on the MoS_2 FETs with 1T-MoS_2 electrodes [27]. In order to compare the performance of MoS_2 FETs with pure 1T electrodes and locally introduced 1T-MoS_2 electrodes, taking the BAC stacked 1T/2H MoS_2 interfaces as an example, we calculated the total DOS, the PDOS of 2H-MoS_2 and locally introduced 1T-MoS_2 (Figures S6 and S7). It is found that the p-type SBH value (0.49 eV) of 1T/2H MoS_2 with pure 1T-MoS_2 is lower than those of 1T/2H MoS_2 with locally introduced 1T-MoS_2 (0.57 eV). Our above analysis strongly supports Kappera *et al*'s expectation that MoS_2 FETs with pure 1T phase electrodes will have even

greater enhancement in performance than those with locally introduced 1T-MoS_2 electrodes [27].

The pristine 2H-MoS_2 monolayer exhibits a direct band gap at the K point (Figure S4), its CBM is mostly contributed by Mo d_z^2 orbitals, while its VBM is composed of mainly Mo d_{xy} and d_x^2-$_y^2$ orbitals. With increasing the number of layers, the VB edge at Γ point dominated by Mo dz^2 orbitals becomes important and increases rapidly [43]. The similar trend occurs when 1T-MoS_2 is added to 2H-MoS_2 to form 1T/2H MoS_2 interfaces: the VBM of 2H-MoS_2 in all the 1T/2H MoS_2 interfaces is dominated by Mo dz^2 orbitals, instead of Mo d_{xy} and d_x^2-$_y^2$ orbitals as in the pristine 2H-MoS_2 monolayer (figure 3), and is shifted from K point to Γ point (Figure 2). On the other hand, as compared with the pristine 2H-MoS_2 monolayer, in 1T/2H MoS_2 interfaces the conduction bands of 2H-MoS_2 are well preserved with the CBM located at the K point (Figure 2). Clearly, upon the formation of the 1T/2H MoS_2 interfaces, the VB edge at Γ point of the pristine 2H-MoS_2 shifts to the VBM in 1T/2H MoS_2 interfaces, which explains the decrease of the band gap of 2H-MoS_2 (Figure 2(g)) and the achievement of the p-type SBH in the 1T/2H MoS_2 interfaces.

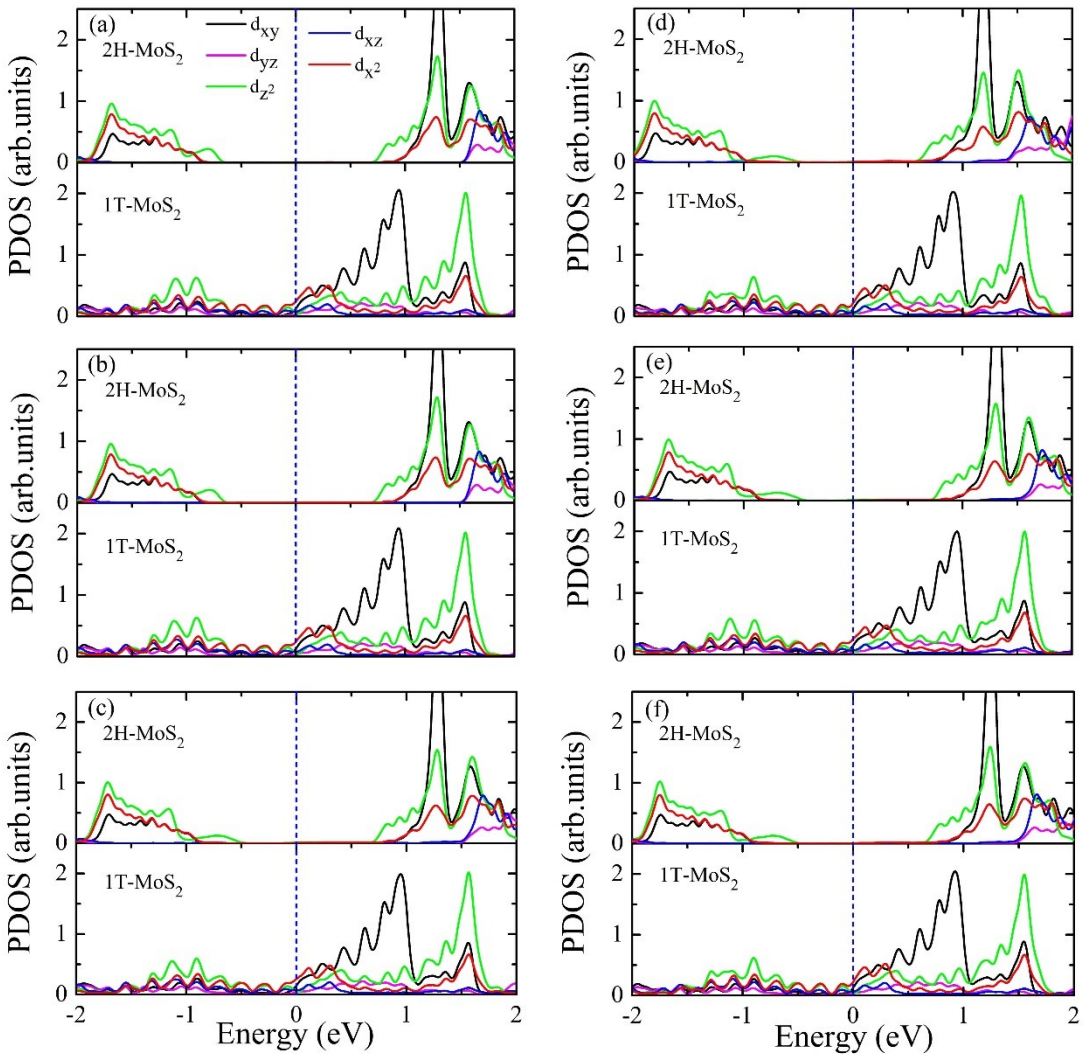

Figure 3. PDOS of 2H-MoS_2 and 1T-MoS_2 in 1T/2H MoS_2 interfaces stacked with (a) ABC, (b) ACB, (c) BAC, (d) BCA, (e) CAB, and (f) CBA, respectively. The top panel is the PDOS of 2H-MoS_2, and the bottom one is the PDOS of 1T-MoS_2. The Fermi level is indicated by the blue dashed lines.

Due to the metallic and semiconducting nature of the 1T and 2H MoS_2 monolayers, the charge transfer between the individual layers in 1T/2H MoS_2 interfaces can be expected. To examine the details of the charge transfer at the 1T/2H MoS_2 interfaces, we investigated the charge difference between the 1T/2H MoS_2

interfaces and the sum of the monolayer 2H-MoS_2 and 1T-MoS_2, i.e, $\Delta\rho = \rho_{1T/2H} - \rho_{1T} - \rho_{2H}$ (Figure S8). To have a quantitative picture, we plotted the plane-averaged electron density difference $\Delta\rho(z)$ along the direction perpendicular to the interface (Figure 4). As shown in Figure 4 (a) and (b), there is only charge depletion at the interfacial region of ABC and ACB stacked 1T/2H MoS_2, similar to metal–graphene contacts [44]. The presence of an interfacial charge depletion region is a direct evidence of the surface charge repulsion effect [45]. Similar to the previous work [45], if there is only charge depletion at the interfacial region between 1T and 2H MoS_2, the antiparallel alignment of interface dipoles will be formed, which would reduce the interface binding energy (as indicated by the black arrows in Figure 4(g)). However, when charge accumulation also occurs at the interfacial region between 1T and 2H MoS_2, the parallel alignment of interface dipoles will be formed, which will contribute to enhance the interface binding energy (as shown in Figure 4(h)). Thus, charge accumulation at the interfacial region could enhance the interface binding energy by tuning the interface dipoles. In contrast, in Figure 4 (c)-(f), the charge accumulation is observed in BAC, BCA, CAB and CBA stacked 1T/2H MoS_2, which suggests a relatively strong interaction between the two monolayers and is consistent with stronger binding energy in BAC, BCA, CAB and CBA stacked 1T/2H MoS_2. Both the charge depletion and the charge accumulation constitute the charge redistribution, leading to the electric dipole formation, or the electrical polarization. Furthermore, in BAC, BCA, CAB and CBA stacked 1T/2H MoS_2 interfaces with charge accumulation, the much stronger charge redistribution implies more

pronounced hybridization and dipole formation at the interface, and consequently larger electrical polarization and striking SBH value difference between these four 1T/2H MoS_2 interfaces (0.44–0.49 eV) and those with only charge depletion at the interfacial region (namely ABC and ACB stacked 1T/2H MoS_2, 0.65–0.67 eV). The above conclusions were further substantiated by the charge difference between the 1T/2H MoS_2 interfaces and the sum of the monolayer 2H-MoS_2 and 1T-MoS_2 (Figure S8).

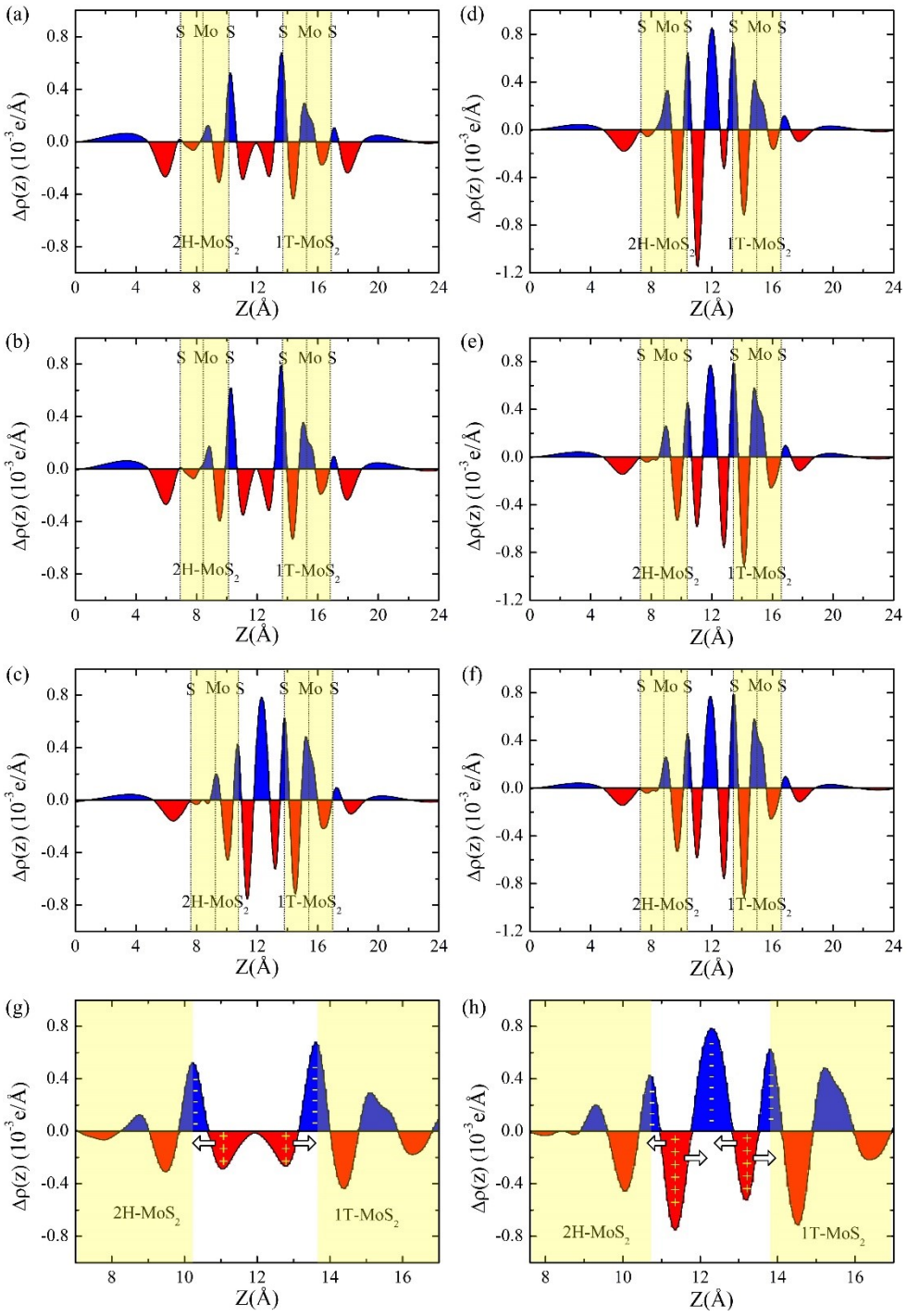

Figure 4. The plane-averaged electron density difference (Δρ(z)) along the direction perpendicular to the interface. (a) ABC, (b) ACB, (c) BAC, (d) BCA, (e) CAB, and (f) CBA stacked 1T/2H MoS_2 interfaces. For each case, the atomic plane positions are given by the dotted lines for reference. The blue and red colors indicate electron accumulation and depletion, respectively. (g) The antiparallel alignment of interface

dipoles in ABC stacked 1T/2H MoS_2 interface, and (h) the parallel alignment of interface dipoles in BAC stacked 1T/2H MoS_2 interface.

An intrinsic electric field can be introduced by the electrical polarization in the 1T/2H MoS_2 interfaces, and previous studies showed that the electronic structures of bilayer MoS_2 can be tuned by vertical electric field [46]. Then, to what extent will the electric field affect the SBH values in the 1T/2H MoS_2 interfaces? To address this question, we applied an external vertical electric field across the interface, and the electric field from 2H-MoS_2 to 1T-MoS_2 was defined as positive. Figure 5 presents the SBH values of the 1T/2H MoS_2 interfaces under various electric fields, in which the red and blue colors indicate n-type and p-type SBH values, respectively. The general trend is clear: under a positive electric field, the n-type SBH consistently increases with increasing electric field, while the p-type SBH generally decreases, eventually achieving a significantly low p-type SBH value of nearly zero for all the 1T/2H MoS_2. In contrast, a different response is observed when a negative electric field is applied. The n-type SBH gradually decreases with increasing a negative electric field, and finally achieves a significantly low n-type SBH value of nearly zero. In comparison, the p-type SBH gradually increases under a negative electric field. Such an external electric-field-dependent band alignment offers a practical route to tune the SBH values.

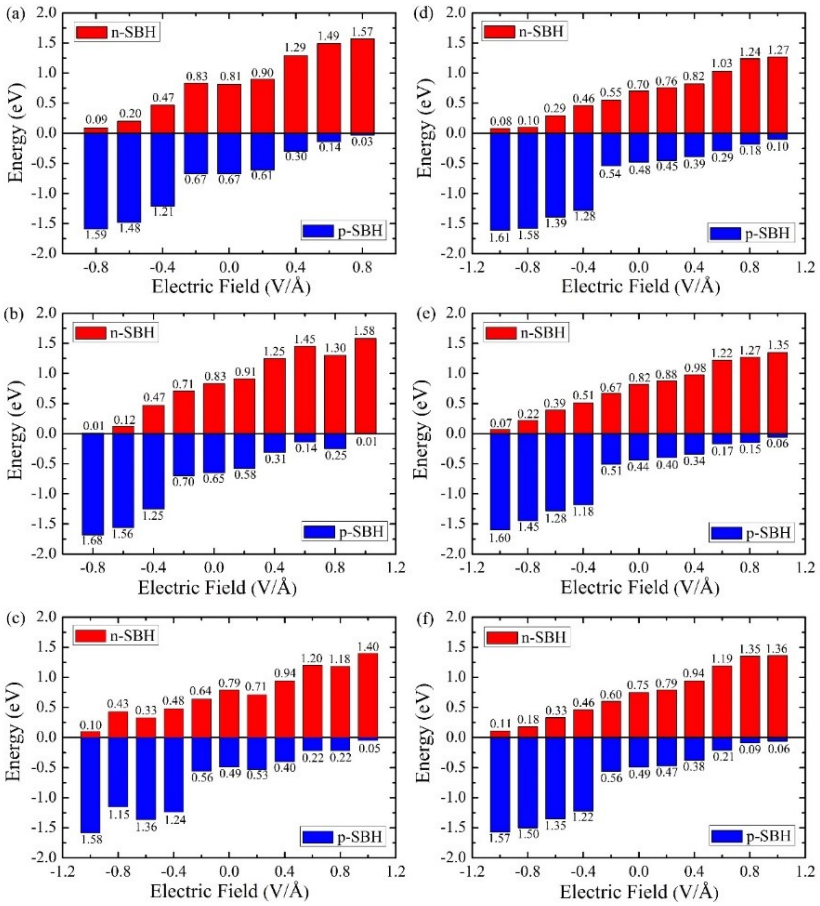

Figure 5. The electric field dependence of the n-type SBH and the p-type SBH values for (a) ABC, (b) ACB, (c) BAC, (d) BCA, (e) CAB, and (f) CBA stacked 1T/2H MoS_2 interfaces. The Fermi level is set at zero. The red and blue colors indicate n-type and p-type SBH values, respectively.

Can our above findings be extended to other 1T/2H TMDs interfaces? To address this question, we examined several other TMDs, such as WS_2, WSe_2 and $MoSe_2$, which have shown significant promise towards realizing p-type FETs [47–49]. Taking the BAC stacked 1T/2H TMDs interfaces as an example, we calculated their band structures, as shown in Figure 6(a)-(c). The p-type SBH values (0.41, 0.66 and 0.74 eV) are lower than their corresponding n-type SBH values (0.99, 0.69 and 0.78 eV),

respectively. Furthermore, we also examined the other five stacking 1T/2H TMDs interfaces, their n-SBH and p-SBH values (Table S1, Supporting Information) clearly showed that the p-type contacts are obtained in these 1T/2H interfaces. By analyzing the band alignment of monolayer 2H-WS_2, 2H-WSe_2, 2H-$MoSe_2$ and the work function of monolayer 1T-WS_2, 1T-WSe_2, 1T-$MoSe_2$ (Figure 6(g)), we found that the work function of 1T-TMDs is closer to the VBM than to the CBM of 2H-TMDs, suggesting that 1T-TMDs can be used as a hole contact for 2H-TMDs. These computational results clearly demonstrate that using 1T phase as an efficient hole injection layer most likely is a universal approach to achieve p-type contacts for other TMDs (such as WS_2, WSe_2 and $MoSe_2$).

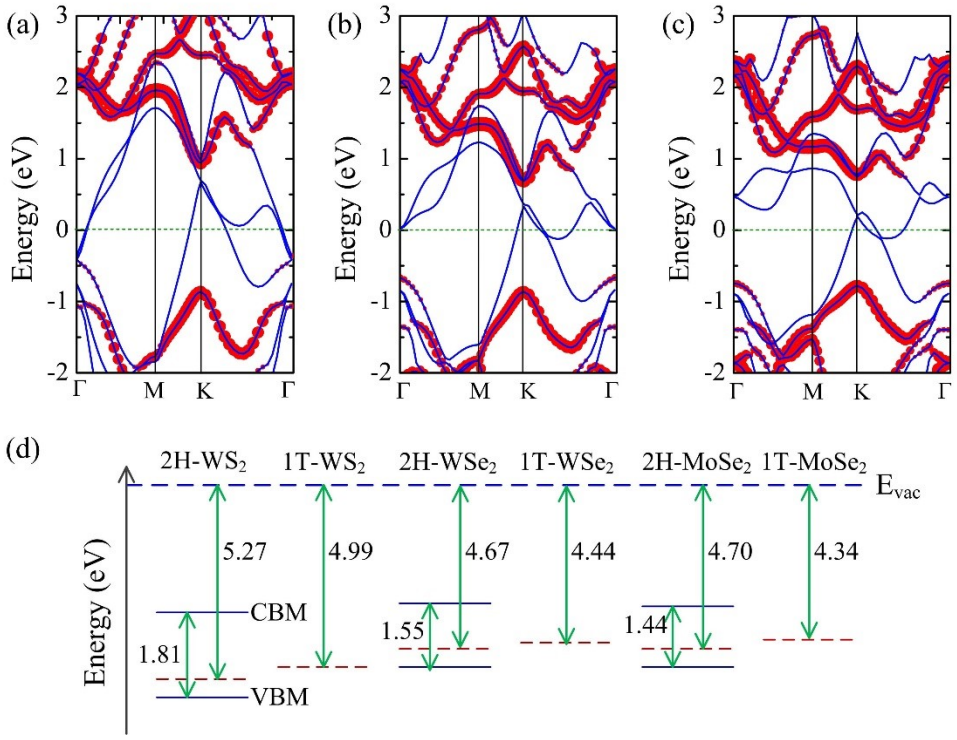

Figure 6. Band structures of 1T/2H TMD interfaces with BAC stacking in (a) WS_2, (b) WSe_2, and (c) $MoSe_2$, respectively. The blue solid lines are the overall band structures. The red dots denote the projected band structures of the 2H-TMD layer. The weight is

represented by the dot size. The Fermi level is set at zero, indicated by the olive dashed lines. (d) Band alignments of monolayer 2H-WS_2, 2H-WSe_2, 2H-$MoSe_2$ and the work function of monolayer 1T-WS_2, 1T-WSe_2, 1T-$MoSe_2$. The red dashed lines are the Fermi level. The vacuum level is taken as reference.

Conclusion

In summary, by means of comprehensive DFT calculations, we investigated carrier injection at the 1T/2H MoS_2 interface and demonstrated that the metallic 1T phase can be used as an efficient hole injection layer for 2H-MoS_2. The 1T-MoS_2 monolayer forms a p-type contact with 2H-MoS_2 due to the increase of VBM of 2H-MoS_2 upon the formation of interface and the dipole formation caused by the charge redistribution at 1T/2H MoS_2 interface. Moreover, the p-type SBH values are lower than those of the n-type Au/MoS_2 and Pd/MoS_2 contacts, which result from the efficient hole injection between 1T-MoS_2 and 2H-MoS_2. This can explain the low contact resistance in the MoS_2 FETs with 1T phase electrodes [27]. Our results also strongly support Kappera *et al*'s expectation that MoS_2 FETs with pure 1T phase electrodes will have even greater enhancement in performance than those with locally introduced 1T-MoS_2 electrodes [27]. Notably, the SBH value can be effectively modulated by an external electric field, and a significantly low p-type SBH value can be achieved under an appropriate electric field. We also demonstrated that this approach can be extended to other TMDs, such as WS_2, WSe_2 and $MoSe_2$, thus may open new promising avenues of contact engineering in TMDs.

Acknowledgements

This work is supported in China by the National Natural Science Foundation of China (Nos.11604047, 51672127), the Natural Science Foundation of Jiangsu Province (No. BK20160694), the Priority Academic Program Development of Jiangsu Higher Education Institutions (PAPD), and the open research fund of Key Laboratory of MEMS of Ministry of Education, Southeast University, and in USA by NSF-CREST Center for Innovation, Research and Education in Environmental Nanotechnology (CIRE2N) (Grant Number HRD-1736093). We also thank CSC Finland for generous grants of computer time.

References

[1] Wang Q H, Kalantar-Zadeh K, Kis A, Coleman J N, Strano M S 2012 Electronics and optoelectronics of two-dimensional transition metal dichalcogenides *Nat. Nanotechnol.* **7** 699–712

[2] Allain A, Kang J, Banerjee K, Kis A 2015 Electrical contacts to two-dimensional semiconductors *Nat. Mater.* **14** 1195–1205

[3] Duan X, Wang C, Pan A, Yu R, Duan X 2015 Two-dimensional transition metal dichalcogenides as atomically thin semiconductors: opportunities and challenges *Chem. Soc. Rev*. **44** 8859–8876

[4] Lembke D, Bertolazzi S, Kis A 2015 Single-layer MoS_2 electronics *Acc. Chem. Res.* **48** 100–110

[5] Chhowalla M, Jena D, Zhang H 2016 Two-dimensional semiconductors for

transistors *Nat. Rev. Mater.* **1** 16052

[6] Manzeli S, Ovchinnikov D, Pasquier D, Yazyev O V, Kis A 2017 2D transition metal dichalcogenides *Nat. Rev. Mater.* **2** 17033

[7] Ma Y, Kou L, Li X, Dai Y, Heine T 2016 Two-dimensional transition metal dichalcogenides with a hexagonal lattice: room-temperature quantum spin Hall insulators. *Phys. Rev. B* **93** 035442

[8] Kou L, Frauenheim T, Chen C 2013 Nanoscale multilayer transition-metal dichalcogenides heterostructures: band gap modulation by interfacial strain and spontaneous polarization *J. Phys. Chem. Lett.* **4** 1730−1736

[9] Chuang S et al 2014 MoS_2 p-type transistors and diodes enabled by high work function MoOx Contacts *Nano Lett*. **14** 1337–1342

[10] Liu H, Neal A T, Ye P D 2012 Channel length scaling of MoS_2 MOSFETs *ACS Nano* **6** 8563−8569

[11] Qiu H, Pan L, Yao Z, Li J, Shi Y, Wang X 2012 Electrical characterization of back-gated bi-layer MoS_2 field-effect transistors and the effect of ambient on their performances *Appl. Phys. Lett.* **100** 123104

[12] Kim S et al 2012 High-mobility and low-power thin-film transistors based on multilayer MoS_2 crystals *Nat. Commun.* **3** 1011

[13] Lemme M C, Li L, Palacios T, Schwierz F 2014 Two-dimensional materials for electronic applications *MRS Bulletin* **39** 711–718

[14] Fontana M, Deppe T, Boyd A K, Rinzan M, Liu A Y, Paranjape M, Barbara P 2013 Electron-hole transport and photovoltaic effect in gated MoS_2 schottky

junctions *Sci. Rep.* **3** 1634

[15] McDonnell S, Azcatl A, Addou R, Gong C, Battaglia C, Chuang S, Cho K, Javey A, Wallace R M 2014 Hole contacts on transition metal dichalcogenides: interface chemistry and band alignments *ACS Nano* **8** 6265–6272

[16] Mak K F, Lee C, Hone J, Shan J, Heinz T F 2010 Atomically thin MoS_2: a new direct-gap semiconductor *Phys. Rev. Lett.* **105** 136805

[17] Radisavljevic B, Radenovic A, Brivio J, Giacometti V, Kis A 2011 Single-layer MoS_2 transistors *Nat. Nanotechnol.* **6** 147–150

[18] Gong C, Colombo L, Wallace R M, Cho K 2014 The unusual mechanism of partial fermi level pinning at metal-MoS_2 interfaces *Nano Lett.* **14** 1714–1720

[19] Chen W, Santos E J G, Zhu W G, Kaxiras E, Zhang Z Y 2013 Tuning the electronic and chemical properties of monolayer MoS_2 adsorbed on transition metal substrates *Nano Lett* **13** 509−514

[20] Zhong H et al 2016 Interfacial properties of monolayer and bilayer MoS_2 contacts with metals: beyond the energy band calculations. *Sci. Rep*. **6** 21786

[21] Musso T, Kumar P V, Foster A S, Grossman J C 2014 Graphene oxide as a promising hole injection layer for MoS_2-based electronic devices *ACS Nano* **8** 11432–11439

[22] Eda G, Chhowalla M 2010 Chemically derived graphene oxide: towards large-area thin-film electronics and optoelectronics *Adv. Mater.* **22** 2392–2415

[23] Voiry D, Mohite A, Chhowalla M 2015 Phase engineering of transition metal dichalcogenides *Chem. Soc. Rev.* **44** 2702–2712

[24] Lin Y, Dumcenco D O, Huang Y, Suenaga K 2014 Atomic mechanism of the semiconducting-to-metallic phase transition in single-layered MoS_2 *Nat. Nanotechnol*. **9** 391−396

[25] Kretschmer S, Komsa H, Boggild P, Krasheninnikov A V 2017 Structural transformations in two-dimensional transition-metal dichalcogenide MoS_2 under an electron beam: insights from first-principles calculations *J. Phys. Chem. Lett.* **8** 3061–3067

[26] Kim J S et al 2016 Electrical transport properties of polymorphic MoS_2 *ACS Nano* **10** 7500−7506

[27] Kappera R, Voiry D, Yalcin S E, Branch B, Gupta G, Mohite A D, Chhowalla M 2014 Phase-engineered low-resistance contacts for ultrathin MoS_2 transistors *Nat. Mater.* **13** 1128−1134

[28] Chhowalla M, Shin H S, Eda G, Li L J, Loh K P, Zhang H 2013 The chemistry of two-dimensional layered transition metal dichalcogenide nanosheets *Nat. Chem.* **5** 263–275

[29] Eda G, Fujita T, Yamaguchi H, Voiry D, Chen M W, Chhowalla M 2012 Coherent atomic and electronic heterostructures of single-layer MoS_2 *ACS Nano* **6** 7311–7317

[30] Lukowski M A, Daniel A S, Meng F, Forticaux A, Li L, Jin S 2013 Enhanced hydrogen evolution catalysis from chemically exfoliated metallic MoS_2 nanosheets *J. Am. Chem. Soc.* **135** 10274 –10277

[31] Wang L, Liu X, Luo J, Duan X, Crittenden J, Liu C, Zhang S, Pei Y, Zeng Y,

Duan X 2017 Self-optimization of the active site of molybdenum disulfide by an irreversible phase transition during photocatalytic hydrogen evolution *Angew. Chem. Int. Ed.* **56** 7610-7614

[32] Kappera R et al 2014 Metallic 1T phase source/drain electrodes for field effect transistors from chemical vapor deposited MoS_2 *APL Mater*. **2** 092516

[33] Kresse G, Furthmüller J 1996 Efficient iterative schemes for ab initio total-energy calculations using a plane-wave basis set *Phys. Rev. B* **54** 11169–11186

[34] Kresse G, Furthmuller J 1996 Efficiency of ab initio total energy calculations for metals and semiconductors using a plane-wave basis set *Comput. Mater. Sci.* **6** 15–50

[35] Blöchl P E 1994 Projector augmented-wave method *Phys. Rev. B* **50** 17953–17979

[36] Kresse G, Joubert D 1999 From ultrasoft pseudopotentials to the projector augmented-wave method *Phys. Rev. B* **59** 1758–1775

[37] Perdew J P, Burke K, Ernzerhof M 1996 Generalized gradient approximation made simple *Phys. Rev. Lett.* **77** 3865–3868

[38] Grimme S 2006 Semiempirical GGA-type density functional constructed with a long-range dispersion correction *J. Comput. Chem.* **27** 1787–1799

[39] Bučko T, Hafner J, Lebègue S, Ángyán J G 2010 Improved description of the structure of molecular and layered crystals: ab-initio DFT calculations with van der Waals corrections *J. Phys. Chem. A* **114** 11814–11824

[40] Gao G, Jiao Y, Ma F, Jiao Y, Waclawik E, Du A 2015 Charge mediated semiconducting-to-metallic phase transition in molybdenum disulfide monolayer and hydrogen evolution reaction in new 1T′ Phase *J. Phys. Chem. C* **119** 13124–13128

[41] Kan M, Wang J Y, Li X W, Zhang S H, Li Y W, Kawazoe Y, Sun Q, Jena P 2014 Structures and phase transition of a MoS_2 monolayer *J. Phys. Chem. C* **118** 1515–1522

[42] Liu Y et al 2015 Toward barrier free contact to molybdenum disulfide using graphene electrodes *Nano Lett.* **15** 3030–3034

[43] Padilha J E, Peelaers H, Janotti A, Van de Walle C G 2014 Nature and evolution of the band-edge states in MoS_2: from monolayer to bulk *Phys. Rev. B* **90** 205420

[44] Gong C, Lee G, Shan B, Vogel E M, Wallace R M, Cho K 2010 First-principles study of metal-graphene interfaces *J. Appl. Phys*. **108** 123711

[45] Gong C, Hinojos D, Wang W, Nijem N, Shan B, Wallace R M, Cho K, Chabal Y J 2012 Metal–graphene–metal sandwich contacts for enhanced interface bonding and work function control *ACS Nano* **6** 5381–5387

[46] Liu Q, Li L, Li Y, Gao Z, Chen Z, Lu J 2012 Tuning electronic structure of bilayer MoS_2 by vertical electric field: a first-principles investigation *J. Phys. Chem. C* **116** 21556–21562

[47] Fang H, Chuang S, Chang T C, Takei K, Takahashi T, Javey A 2012 High-performance single layered WSe_2 p-FETs with chemically doped contacts *Nano Lett.* **12** 3788

[48] Chuang H, Chamlagain B, Koehler M, Perera M M, Yan J, Mandrus D, Tomnek D, Zhou Z 2016 Low-resistance 2D/2D ohmic contacts: a universal approach to high-performance WSe_2, MoS_2, and $MoSe_2$ transistors *Nano Lett.* **16** 1896

[49] Huang L, Zhong M, Wei Z, Li J 2017 Tunable schottky barrier at $MoSe_2$/metal interfaces with a buffer layer *J. Phys. Chem. C* **121** 9305–9311